Composites Science and Technology xxx (2009) xxx–xxx

Contents lists available at ScienceDirect

Composites Science and Technology

journal homepage: www.elsevier.com/locate/compscitech

Interlaminar and intralaminar reinforcement of composite laminates with aligned carbon nanotubes

Sunny S. Wicks *, Roberto Guzman de Villoria, Brian L. Wardle

Dept. of Aeronautics and Astronautics, Massachusetts Institute of Technology, Cambridge, MA 02139, USA

ARTICLE INFO

Article history:
Received 13 July 2009
Received in revised form 31 August 2009
Accepted 2 September 2009
Available online xxxx

Keywords:
A. Hybrid composites
A. Carbon nanotubes
B. Fracture toughness
B. Mechanical properties
B. Strength

ABSTRACT

Three-dimensional reinforcement of woven advanced polymer–matrix composites using aligned carbon nanotubes (CNTs) is explored experimentally and theoretically. Radially-aligned CNTs grown *in situ* on the surface of fibers in a woven cloth provide significant three-dimensional reinforcement, as measured by Mode I interlaminar fracture testing and tension-bearing experiments. Aligned CNTs bridge the ply interfaces giving enhancement in both initiation and steady-state toughness, improving the already tough system by 76% in steady state (more than 1.5 kJ/m^2 increase). CNT pull-out on the crack faces is the observed toughening mechanism, and an analytical model is correlated to the experimental fracture data. In the plane of the laminate, aligned CNTs enhance the tension-bearing response with increases of: 19% in bearing stiffness, 9% in critical strength, and 5% in ultimate strength accompanied by a clear change in failure mode from shear-out failure (matrix dominated) without CNTs to tensile fracture (fiber dominated) with CNTs.

1. Introduction

Carbon nanotubes continue to interest researchers for their exceptional mechanical, thermal, and electrical properties. While amply demonstrated on the nanoscale, taking advantage of intrinsic (and even scale-dependent) properties in macroscale structural systems presents significant challenges. A promising structural application for CNTs is reinforcement of traditional fiber-reinforced plastic (FRP) advanced composites [1–6]. In traditional composites, properties are tailored by controlling the direction of the reinforcing fibers as in a unidirectional composite. Aligned CNTs are envisioned as a second, albeit nanoscale, fiber that can be combined within the microscopic framework of existing FRPs to create hybrid, or nano-engineered, composites [7–11]. A particular focus for reinforcement with aligned CNTs is the interface between FRP plies, a region well known as a 'weak link' in laminated composites. The interlaminar region is devoid of fiber reinforcement and fails via various modes, primarily delamination and matrix cracking, which may develop during the service life of the structure. Relatively poor interlaminar properties severely limit the overall performance of advanced laminated composites systems. Several solutions have emerged to strengthen the interface: 3D-textiles, stitching, and z-pinning, all of which reinforce the composite in the through-thickness (composite *z*-axis) direction with typically micron-diameter advanced fibers in bundles or pins with lengths on the order of millimeters [12–20]. The primary and unaddressed drawback of these existing solutions is that there is an unavoidable, and typically significant, reduction of in-plane mechanical properties due to lamina and laminate damage and in-plane fiber volume loss, e.g., lamina fiber and matrix damage due to *z*-direction pin insertion [12,18,21,22].

Due to their size, nanoscale fibers such as CNTs can be introduced into the polymer matrix region (order of 1 μm spacing) between existing micron-diameter fibers to reinforce the laminate. Work by others with CNTs and other nanomaterials has either focused solely on the interlaminar area, or has dispersed small quantities (by volume) of unaligned CNTs within the matrix via mixing or other methods for intralaminar reinforcement. Due to significant issues such as agglomeration, lack of alignment, poor dispersion, and damage to CNTs during mixing, only marginal mechanical property improvements are observed for both nanocomposites [23] and hybrid composites [24–26] when CNTs are mixed into the bulk matrix. Somewhat more success has been achieved with nanoscale modification of the interlaminar region (between plies), either by growing CNTs on the surface of cloth [27] or placing unaligned CNTs at low volume fraction at the interface [28–31]. An area of particular activity has been in growing CNTs on the surface of carbon fibers to reinforce carbon FRP (CFRP), with the additional unfortunate difficulty that typical CNT growth processes significantly damage tensile properties of the carbon fibers [32–35].

Here, aligned CNTs are introduced in *both* the interlaminar and intralaminar regions of the laminate, providing three-dimensional reinforcement (see Fig. 1). This architecture has been introduced previously into the literature as a fuzzy fiber-reinforced plastic

* Corresponding author. Tel.: +1 617 252 1539; fax: +1 617 253 0361.
E-mail address: wardle@mit.edu (S.S. Wicks).

0266-3538/$ - see front matter © 2009 Elsevier Ltd. All rights reserved.
doi:10.1016/j.compscitech.2009.09.001

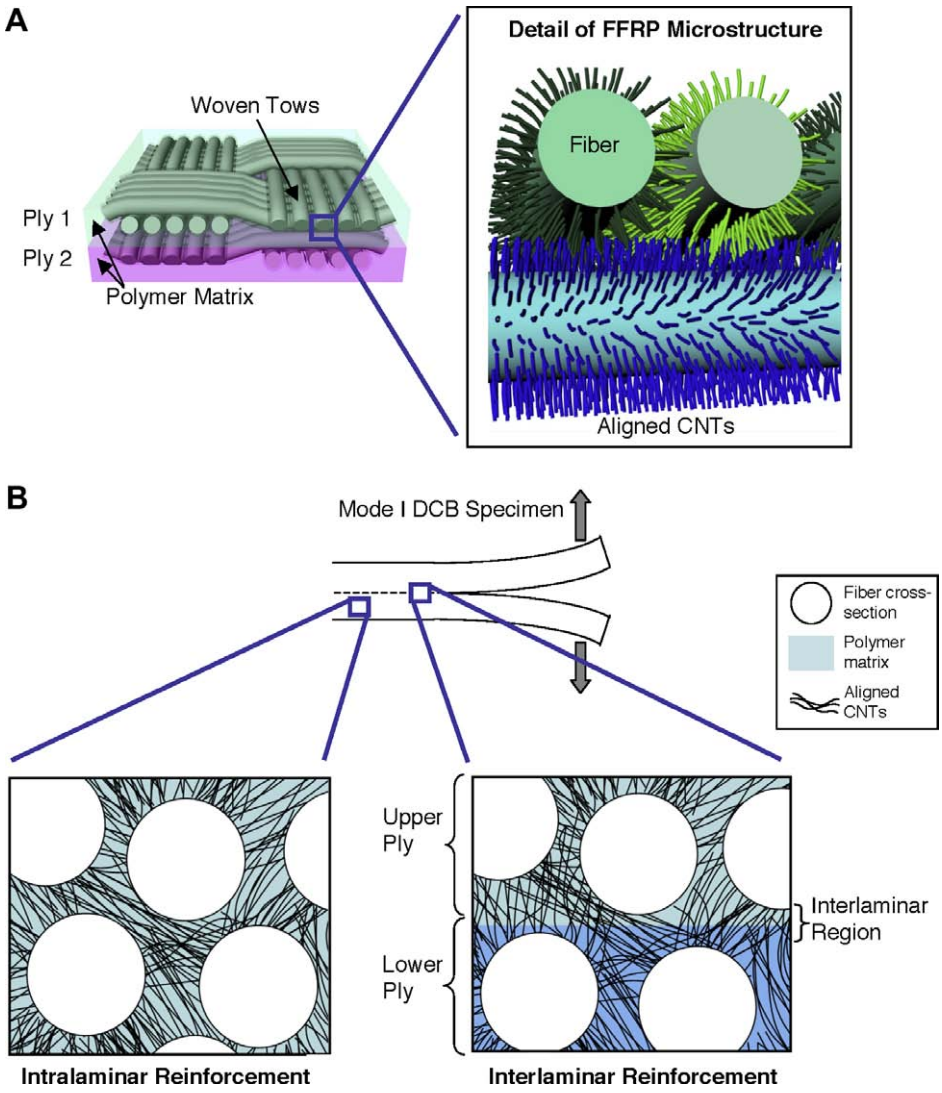

Fig. 1. Illustration of fuzzy-fiber-reinforced plastic (FFRP). (A) Radially-aligned CNTs grown on advanced fiber cloth. (B) CNT intralaminar and interlaminar reinforcement.

(FFRP) laminate [10]. Prior work with this architecture has shown property enhancement due to the aligned CNTs (interlaminar shear strength as measured by short-beam shear increased ~70%, and electrical conductivity increased by more than 10^6). Due to advances in larger-scale synthesis [36], the work here investigates the magnitude and mechanisms of Mode I interlaminar toughness and tension-bearing strength enhancement. Significant toughness enhancement observed in steady-state is attributed to CNT-pull-out toughening, or bridging, consistent with observations of CNT pull-out from crack surface inspection. Bridging is modeled using a recently developed analytical approach [37] and shown to predict the magnitude of observed toughening. Aligned CNTs in the FFRP architecture also reinforce the intralaminar region of the laminate. In-plane strength and stiffness enhancement due to the aligned CNTs is assessed via a standard through-hole tension-bearing strength testing. Tension-bearing strength is a critical property for composites given the pervasive use of mechanical fasteners, and the poor performance of composites relative to metals in this area [38]. Thus, the effectiveness of aligned CNTs in providing intralaminar and interlaminar reinforcement between fibers and between plies is assessed in this work for the FFRP architecture, building on the prior observed positive interlaminar shear strength improvement assessed via short-beam-shear (SBS) testing [10].

2. Experimental

Fabrication and characterization of the specimens is described including CNT synthesis, laminate fabrication, and characteristics of the laminates, followed by details of the Mode I fracture and tension-bearing testing.

2.1. Aligned-CNT growth and characterization

Fabrication of the fuzzy-fiber plies for the FFRP composites involves growing CNTs directly on fibers in an alumina fiber woven cloth using a modified thermal chemical vapor deposition (CVD) method developed in previous work [7,8]. Commercially available thick (900 g/m^2, ~1 mm thick) alumina fiber cloth woven in a 0°/90° satin-weave was used as the base composite fiber, as it is compatible with the particular CNT growth chemistry employed and because it has been recently optimized for large-area uniform three-dimensional growth needed for the ASTM-standard Mode I specimens [36]. The alumina fibers are ~11 μm in diameter, and each tow consists of 3000 fibers, yielding a dry alumina cloth volume fraction of approximately 65%. The CNT growth process has been shown not to affect tensile properties of the alumina fibers

Please cite this article in press as: Wicks SS et al. Interlaminar and intralaminar reinforcement of composite laminates with aligned carbon nanotubes. Compos Sci Technol (2009), doi:10.1016/j.compscitech.2009.09.001

[7,8]. Alumina FRP composites have been studied previously for enhanced strength at low-temperatures (over glass-thermoset systems) [39], and currently in integral armor [40] concepts.

Alumina cloth is first soaked in a solution of 50 mM iron nitrate in isopropanol for 5 min and dried in air for at least 8 h. This catalyst application method allows the catalyst to coat fibers inside the tows of the ply. In an atmospheric pressure CVD furnace, the 15 cm by 4.5 cm cloth (see Fig. 2) is heated and held stable for 7 min in a reducing environment at 650 °C to condition the catalyst to form nanoparticles that initiate CNT growth. With the introduction of ethylene feedstock gas, CNTs grow in a radially-aligned (alumina fiber axis) morphology perpendicular to the surface of the fibers. Further details of the growth process have been published previously, including the effect of CNT length on the morphology of growth [36]. The aligned CNTs are sufficiently long (20–30 μm) to span interply matrix regions, and have a "mohawk"-type of morphology where the aligned CNTs group into microscopic bundles on the surface of the fibers at lengths greater than ~1 μm [36]. By growing CNTs directly on the fibers, the resulting distribution is considerably more uniform than can be achieved by other dispersion methods and, just as importantly, CNT alignment and high volume fraction are established [10]. Optical and SEM characterization reveals high-yield aligned-CNT growth (see Fig. 2), and TEM imaging reveals a multi-walled CNTs (MWCNT) having an average diameter of ~14 nm with eight walls (see example in Fig. 2A).

2.2. Composite manufacturing and characterization

FFRP and baseline plies are fabricated into laminates using hand lay-up for Mode I and tension-bearing testing. The matrix system used is West Systems Epoxy, Resin 105 and Hardener 206. Each ply is placed on a sheet of non-porous Teflon, and de-gassed room-temperature epoxy is applied. The epoxy is drawn into the interior of the woven ply within a few seconds and then another ply is added. Aligned-CNT forests wet easily through capillary forces that draw the polymer into the forest [41], and this mechanism is used to fabricate the FFRP laminates here [10,42,43]. Plies are then stacked with appropriate cure materials, and vacuum is used to consolidate the laminate. Samples are then left to cure for at least 12 h at room temperature. After curing, specimens are trimmed using a diamond-grit wet cutting wheel. The resulting specimens have less than 2% void fraction in all cases (including FFRP and baseline specimens) and fiber volume fraction of 50%. CNT and fiber volume fraction are calculated from measured mass and volume of the samples following the simple procedures detailed elsewhere [36], and void fraction is calculated from optical microscope images of specimen cross-sections along the length of each fabricated specimen.

Mode I FFRP specimens (see Figs. 2 and 3) utilize two fuzzy-fiber plies between two baseline plies in order to conserve the number of CNT-grown plies, noting that the fracture behavior of interest is along the laminate centerline. A thin-film Teflon layer is placed along the centerline on the last 50.8 mm (2″) of the laminate to form an initial precrack. Chopped fiberglass plates were bonded on both surfaces of the sample to stiffen the specimen and prevent bending failure following a technique developed for stitched specimens that have high interlaminar toughness [15,27,44,45]. Hinges were then attached to the fiberglass using epoxy adhesive (JBWeld) to facilitate load transfer during testing. An annotated image of an FFRP Mode I specimen is shown in Fig. 3. The overall size of a completed specimen is 25.4 mm (1″) wide by 152.4 mm (6″) long, and 6 of the FFRP laminates and 4 of the baseline laminates were fabricated and tested. For the tension-bearing test specimens, 3 each of baseline and FFRP plates

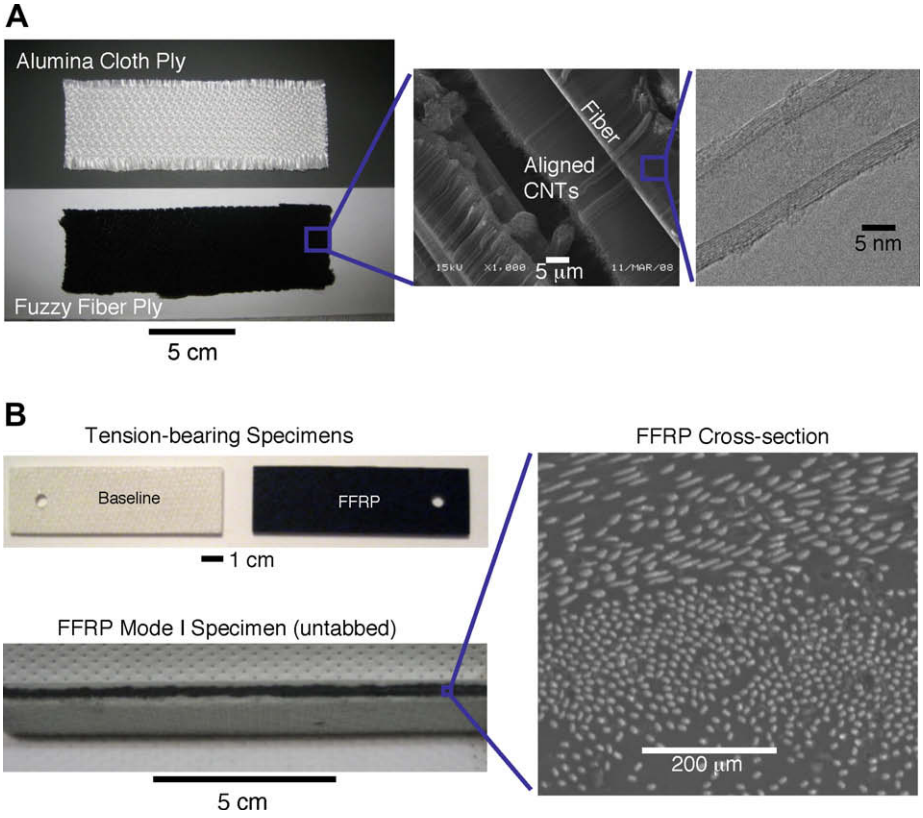

Fig. 2. Sample fabrication. (A) A baseline alumina ply and a fuzzy fiber ply after CNT growth, including SEM of aligned CNTs and TEM image of an individual CNT. (B) Laminates for Mode I fracture and tension-bearing testing.

Please cite this article in press as: Wicks SS et al. Interlaminar and intralaminar reinforcement of composite laminates with aligned carbon nanotubes. Compos Sci Technol (2009), doi:10.1016/j.compscitech.2009.09.001

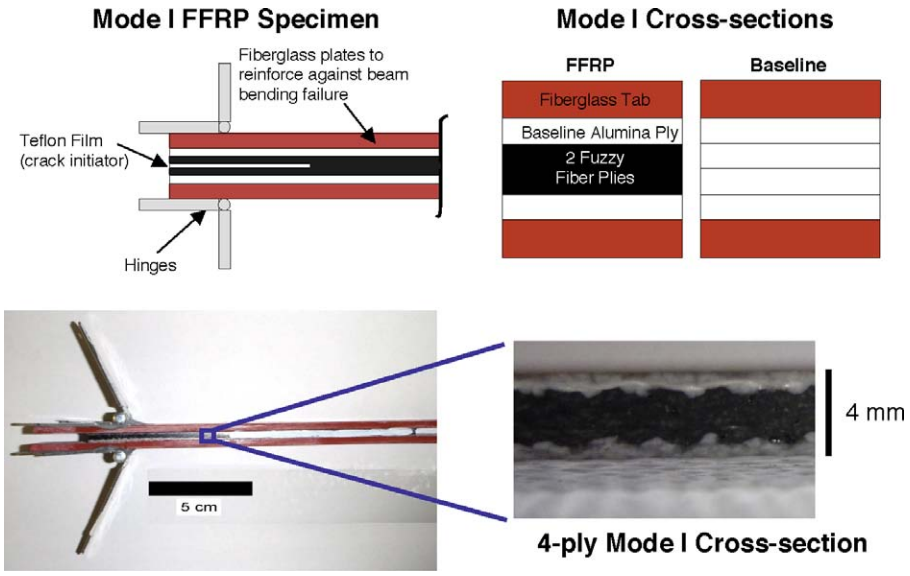

Fig. 3. Illustration and images of Mode I fracture specimens.

are trimmed to 108.0 mm long, 3 mm thick (three plies) and 31.8 mm wide. A 6.35 mm (1/4″) diameter hole was drilled with a diamond-grit core drill at 15.9 mm (5/8″) from the specimen top edge, as shown in Fig. 2B.

2.3. Mode I fracture and tension-bearing mechanical testing

Mode I fracture testing and data reduction follows ASTM D-5528. Hinged Mode I specimens were loaded at 2 mm/min until 100 N was reached, followed by continued loading at 0.5 mm/min. Crack propagation began at the end of the 50.8 mm (2″) long Teflon layer and data was taken at the visual onset of the crack and for every millimeter thereafter. Load, crack length, and arm displacement as a function of time were recorded. The results of these measurements are used to determine R-curves that are used to assess toughness of these hybrid composites [46,47] using the compliance calibration method [46]. Initiation toughness is calculated using both the visual onset and nonlinear method, and steady-state toughness is determined directly from the full R-curve. Specimen fracture surfaces are characterized *post mortem* by optical and scanning electron microscopy (SEM).

Single-shear bearing tests were carried out in a uniaxial testing machine. A steel fixture designed for single shear is attached to the specimen hole by means of a 6.35 mm (1/4″) diameter steel pin (see Fig. 6). The specimen was loaded in tension at 0.25 mm/min. In order to monitor hole deformation during the test, a crack opening displacement (COD) gage is placed across the hole following the recommendations of the standard [48]. Far-field applied strain is measured via back-to-back standard strain gages. Specimens before and after testing are characterized via optical and scanning electron microscopy (SEM).

3. Results and discussion

Mode I experimental fracture results are first presented and then interpreted using a recently developed analytical fracture model for *z*-direction (including CNTs) reinforced interfaces. Results from tension-bearing testing are then presented to assess in-plane (intralaminar reinforcement) due to the *z*-direction interlaminar reinforcement.

3.1. Mode I interlaminar fracture toughness

Reduction of the test data and R-curves for all specimens tested (baseline and FFRP) yields well-behaved resistance- (R-) curves showing the critical initiation toughness ($G_{Ic,\,i}$) leading to steady-state (propagation) toughness ($G_{Ic,\,ss}$) as shown in the representative R-curves in Fig. 4. There is little variation along the progression of the R-curve in steady-state as is sometimes noted in testing of some laminated composite systems [46,47]. Two values of initiation toughness (visual, $G_{Ic,\,i\text{-}vis}$, and nonlinear, $G_{Ic,\,i\text{-}nl}$) are calculated based on the Standard, with the nonlinear being considered conservative [46]. Table 1 contains a summary of the reduced fracture data for all specimens tested, and allows a direct comparison between the baseline (no CNTs) and FFRP (CNTs) response. Due to the aligned CNTs, initiation toughness increases by more than 60% and steady-state toughness increases by 76%. The baseline laminate is a woven system and would be considered a very tough interface having $G_{Ic,\,ss}$ of greater than 2 kJ/m^2 (by comparison, most aerospace epoxy-based laminate systems have $G_{Ic,\,ss}$ of less than 0.5 kJ/m^2). Woven composites inherently have higher fracture toughness than unidirectional prepreg-based systems (0.1–0.3 kJ/m^2). This is due to increased fracture surface area and 90° fibers working as built-in crack arrestors [49]. $G_{Ic,\,ss}$ toughness for the CNT-reinforced specimens reaches nearly 4 kJ/m^2, which is in the range of toughness (4–6 kJ/m^2) for z-pin and stitching reinforcement at stitch densities (1%) [22] comparable to the CNTs in the FFRP. The CNTs act as interlaminar (short) 'nanostitches' to reinforce the laminate, without the significant detrimental effects on in-plane properties due to damage from stitch and z-pin insertion [12].

Evaluation of the fracture surfaces of the specimens indicates a similar microscopic fracture surface morphology (following the weave of the cloth) for the baseline and FFRP specimens. However, in the FFRP fracture surfaces, CNTs are observed to extend from both sides of the crack face (see examples in Fig. 4). Thus, the microscale fracture behavior seems to be unchanged but a new nanoscale feature is observed under SEM. It should be noted that optical and SEM evaluation indicates no difference in the thickness of the interlaminar region between the two fuzzy-fiber plies vs. the baseline specimen. This is not surprising given the coarse weave and rather short lengths of the CNTs relative to the tow diameters. The bridging behavior of the CNTs (CNT pull-out length is 3–7 μm)

Please cite this article in press as: Wicks SS et al. Interlaminar and intralaminar reinforcement of composite laminates with aligned carbon nanotubes. Compos Sci Technol (2009), doi:10.1016/j.compscitech.2009.09.001

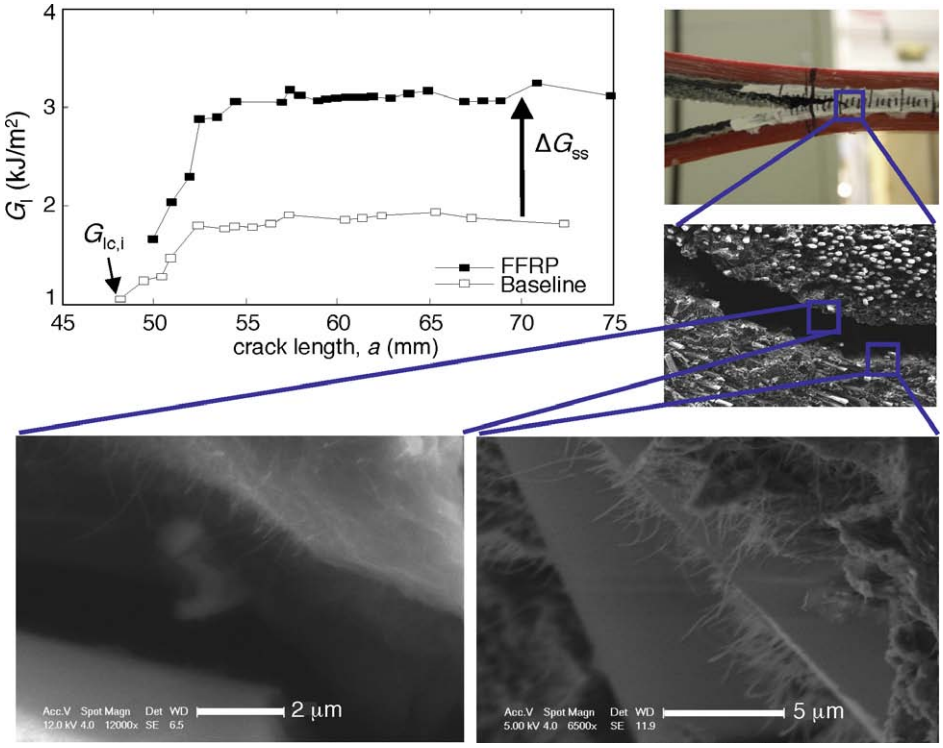

Fig. 4. Representative R-curves from Mode I tests and SEM images of fracture surface exhibiting CNT pull-out.

Table 1
Summary data for Mode I fracture tests.

Material	Alumina V_f (%)	CNT V_f (%)	Nonlinear initiation fracture toughness, $G_{Ic,\ i\text{-}nl}$ (kJ/m^2)	Visual initiation fracture toughness, $G_{Ic,\ i\text{-}vis}$ (kJ/m^2)	Steady-state fracture toughness, $G_{Ic,\ ss}$ (kJ/m^2)
Alumina/epoxy	53	0.0	1.21 ± 0.07	1.27 ± 0.21	2.12 ± 0.15
FF/epoxy	50	1–2	2.02 ± 0.32	2.07 ± 0.28	3.74 ± 0.82
Change	–	–	+67%	+63%	+76%

is apparent in Fig. 4, where CNTs are observed extending into the crack path, indicating that CNTs were pulled out of the matrix and/or fractured. No statistical difference was seen between the crack length of baseline and FFRP laminates when steady-state fracture toughness was reached. This suggests that bridging from the micron-diameter fibers (and tows) occurs in both the baseline and FFRP composites, with CNTs in the FFRP adding toughness. CNTs add both matrix toughening and CNT bridging toughening in the FFRP specimens, unlike z-pinning and stitching that are completely ineffective at resisting initiation and growth of short delaminations.

3.2. Mode I toughness model-experiment correlation

Toughness enhancement due to the aligned CNTs in the interlaminar region may be attributed to several mechanisms, including mechanical bridging and polymer yielding/crazing [50]. Polymer crazing has been shown to yield impressive relative improvements in neat epoxy (~100% in $G_{Ic,\ ss}$) but relatively small (0.4 kJ/m^2) absolute improvements. However, CNT pull-out has been observed in the FFRP specimens (see Fig. 4 and related discussion), and is modeled here using a previously-developed cohesive zone approach that provides a closed-form expression for toughening due to CNT pull-out [37]. As the crack progresses, the stitches are sequentially slid out of the matrix until they are pulled free. In the case of MWCNTs such as those used here in the FFRP, a sword-in-sheath mechanism is treated in the model, wherein the inner tube of the CNT is pulled out of the external shell [37]. Toughening via the sword-in-sheath mechanism is much less than pull-out toughening due to the low frictional forces between concentric CNTs. Using the J-integral, as developed in [37], improvement in fracture toughness for both pull-out and sword-in-sheath modes can be derived in closed form, in agreement with similar work using a numerical implementation to calculate stress-intensity factors [51,52]. The enhancement in toughness is given by the increment in steady-state toughness ($\Delta G_{Ic,\ ss}$) due to CNT bridging:

$$\Delta G_{Ic,SS} = \frac{1}{2}\left(\frac{L}{r}\right)(v_f \tau L) \tag{1}$$

where L, r, and v_f are the length, radius, and volume fraction of the CNTs pulled out of the matrix, and τ is the interfacial (sliding) shear stress between the reinforcing fiber and the polymer matrix [53]. The pull-out length L in this general analysis may not be the entire CNT length, L_{CNT}, due to CNT fracture as discussed subsequently. The scale dependence of the fiber on toughening, given by the inverse of the aspect ratio, favors small radii fibers such as CNTs. Limiting the toughening is the strength of the reinforcing fiber, which suggests that nanoscale fibers of high strength (such as CNTs) are uniquely ideal bridging elements.

Implementing the model to include characteristics of the FFRP architecture allows prediction of steady-state toughening. Unless otherwise noted, nominal values of these parameters are: r = 7 nm,

Please cite this article in press as: Wicks SS et al. Interlaminar and intralaminar reinforcement of composite laminates with aligned carbon nanotubes. Compos Sci Technol (2009), doi:10.1016/j.compscitech.2009.09.001

L = 10 μm, v_f = 1% (estimated v_f of CNTs in matrix at crack plane), and τ = 10 MPa, (see discussion in [37]). CNT visualization under SEM after crack propagation (see Fig. 4) allows estimation of CNT pull-out length, L, taken to be in the range of 3–7 μm. It is expected that, due to the complex morphology of the fracture surfaces and CNT morphology, multiple toughening mechanisms are operating including toughening due to the woven nature of the plies as discussed in the previous section. Toughening mechanisms inherent to the alumina-fiber weave and epoxy system can be incorporated into the predicted steady-state toughness by observation of toughening in experimental baseline G_{Ic} curves. In the representative curves in Fig. 4, an increase of ~1 kJ/m^2 can be seen between $G_{Ic,\,i}$ and $G_{Ic,\,ss}$ of the baseline (no CNTs) specimen, which would represent an upper-bound increment in toughness due to the weave. Therefore, given an experimental $G_{Ic,\,i}$ of the FFRP laminate of ~1.5 kJ/m^2, toughening of the FFRP system can be predicted using the closed-form solution of CNT bridging (see Fig. 5) with good agreement using the observed CNT pull-out lengths. Similarly, the effects of CNT pull-out length and CNT volume fraction on the predicted steady-state toughness can also be discerned with the model (see Fig. 5). Longer CNTs, higher volume fraction, and higher frictional stress enhance steady-state toughness (see Eq. (1)). However, as mentioned previously, CNT fracture (strength) limits the amount of toughening because a critical point is reached where the CNTs fracture instead of pull-out, yielding less toughening (see change from "pull-out" to "sword-in-sheath" in Fig. 5, right); a relatively low value of CNT (MWCNT) fracture stress of 30 GPa is used that is less than the average of the measured range in the literature [37,54]. The model and the sensitivities in toughness enhancement from Eq. (1) shown in Fig. 5, right, indicate the magnitude of toughening achievable and the routes to achieving it. As an example, recent work has shown several routes to improving mechanical properties of CNTs, particularly MWCNTs, via various routes, e.g., [55–57]. Engineering CNT strength enhancement allows longer CNT lengths to be pulled out of the matrix, thus improving toughness enhancement due to pull-out toughening. This can be considered as in Fig. 5, right, by moving the critical point that separates the (higher) pull-out toughening from the (lower) sword-in-sheath toughening to the right. Doubling of the CNT strength to 60 GPa (a value within the range of reported data [54]), the critical point in the analysis in Fig. 5, right, would move to the right, increasing the range of CNT pull-out length L such that the predicted toughness increases 155% to 15.5 kJ/m^2 at L = 42 μm. Thus, the model can be used to calculate expected improvements to toughness from materials engineering of relevant CNT properties associated with toughening.

It is interesting to note that given the CNTs implemented, the current FFRP system is not far from optimal toughness (vs. the lower values associated with sword-in-sheath toughening). Other mechanisms of reinforcement due to the CNTs beyond fiber bridging include: polymer hysteretic effects such as crazing, CNT fracture, or CNT bending as they are pulled out of the matrix (the CNTs are radially-aligned, not perpendicular to the crack plane, and also are not straight/collimated but rather wavy [58,59]).

3.3. Tension-bearing testing results

Tension-bearing testing is one of the ASTM standard tests used to evaluate mechanically fastened joints in composites [38], a crit-

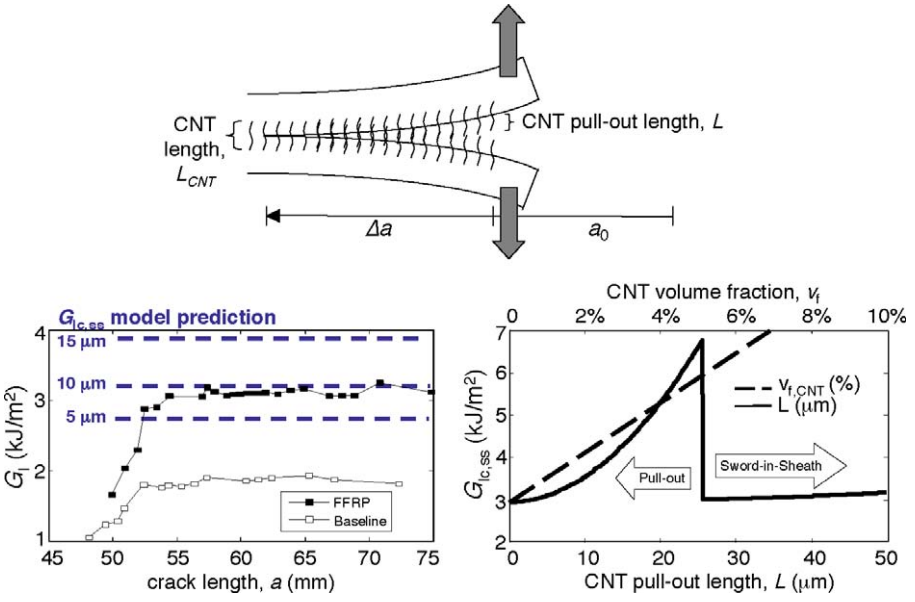

Fig. 5. Experiment-model correlation. Model parameter depiction (top), overlay of $G_{Ic,\,ss}$ prediction with varying CNT pull-out lengths (L) using representative R-curves (left), and dependency of $G_{Ic,\,ss}$ prediction on CNT pull-out length and local volume fraction (right).

Table 2
Summary data from tension-bearing testing.

Material	Alumina fiber V_f (%)	CNT V_f (%)	ASTM D5961 Standard			Literature/industry	
			Chord stiffness, E_{br} (MPa)	(Critical) offset bearing strength, $\sigma_{b\text{-}off}$ (MPa)	Ultimate bearing strength, $\sigma_{b\text{-}ult}$ (MPa)	4% Strength, $\sigma_{4\%}$ (MPa)	Initiation strength, σ_{ini} (MPa)
Baseline	53 ± 3	0.0	25 ± 3	226 ± 8	236 ± 10	103 ± 8	221 ± 21
FFRP	45 ± 1	2.5 ± 0.1	30 ± 6	246 ± 18	248 ± 17	112 ± 20	247 ± 18
Change	–	–	+19%	+9%	+5%	+9%	+12%

Please cite this article in press as: Wicks SS et al. Interlaminar and intralaminar reinforcement of composite laminates with aligned carbon nanotubes. Compos Sci Technol (2009), doi:10.1016/j.compscitech.2009.09.001

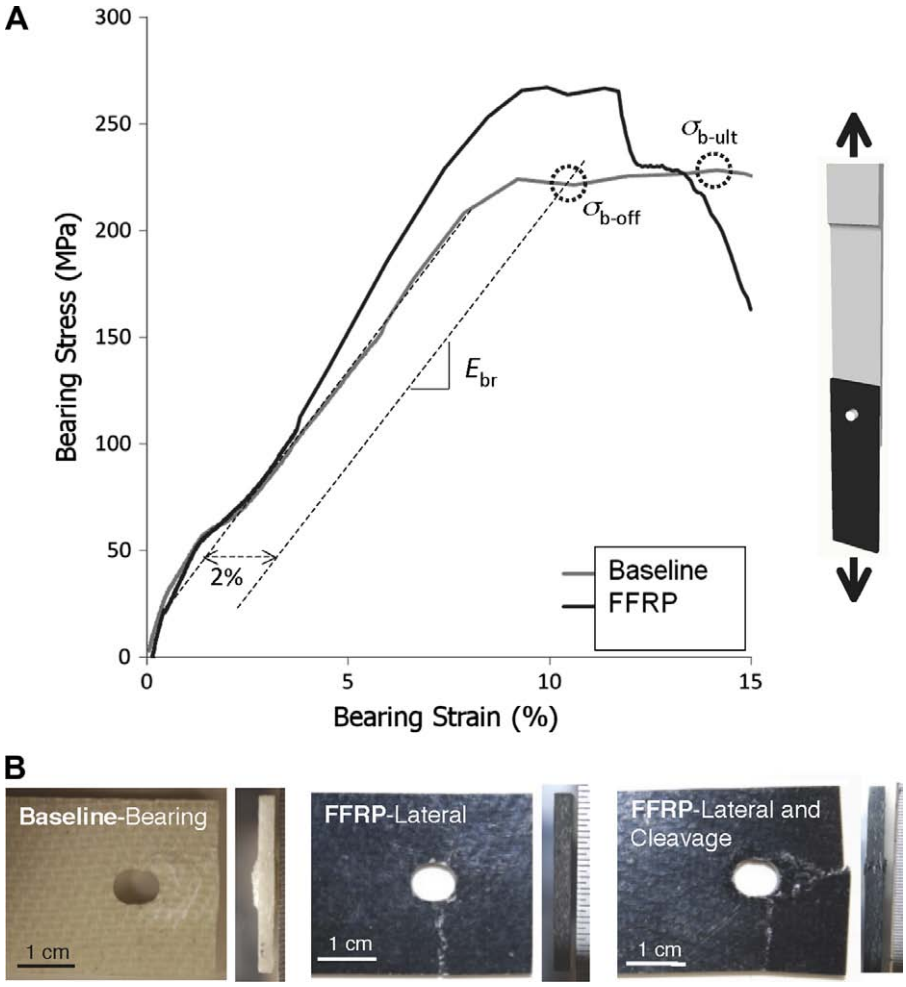

Fig. 6. Tension-bearing testing results: A. Typical bearing stress and bearing strain curve for baseline and FFRP composites. Chord stiffness (E_{br}), initiation strength (σ_{ini}), offset strength ($\sigma_{b\text{-}off}$), and ultimate strength ($\sigma_{b\text{-}ult}$) are indicated on the baseline (no CNTs) curve. B. Lateral (left) and cross-sectional (right) views of bearing failure modes.

ical area for stress transfer and therefore a key application area for new reinforcement solutions. The test is ideally suited for a relative comparison of the behavior of laminates with and without CNTs [48]. The response of the baseline and FFRP laminates is found to be very different, both in terms of critical parameters extracted from the test (see Table 2) and the mode of failure (see Fig. 6). An example bearing-stress vs. bearing-strain response plot is given in Fig. 6A for representative baseline and FFRP specimens, with key points labeled. The stiffness of the sample, as well as both measures of strength, were all enhanced by the presence of the aligned CNTs. Intralaminar reinforcement (see Fig. 1) of the specimen is demonstrated through the significant (19%) bearing stiffness increase, and both intralaminar and interlaminar reinforcement demonstrated through the increases in both strength measures. Other methods for reducing the test data in tension-bearing testing [38,60–62] exist. A common industry method is to calculate bearing strength ($\sigma_{4\%}$) at 4% of bearing strain, and an initial bearing strength (σ_{ini}) determined by the location of the first load drop [38,63,64]. These metrics (see Table 2) show comparable improvement to values reduced using the Standard.

Increases in the bearing properties (stiffness and strengths) due to the aligned CNTs are accompanied by a change in failure mode from a shear-dominated bearing mode without CNTs, to a fiber-dominated fracture mode for the FFRP (see examples in Fig. 6). The Standard characterizes the baseline (no CNT) failure mode as 'Bearing', while the FFRP samples fail in a 'Lateral (Net Tension)' and/or 'Cleavage' mode. The aligned CNTs increase the in-plane stiffness of the laminate (as evidenced by E_{br} increase), but also provide additional through-thickness stiffness, both of which are important in resisting bearing failure in z-pin and stitching reinforcement [65,66]. Visual evidence of *z*-direction (through-thickness) stiffness enhancement is shown by the laminate cross-sections after testing in Fig. 6B. The baseline specimen expands ("bulging of the bearing joint" [67]) in the region of bearing failure, where the aligned-CNT reinforced specimen has significantly less expansion in the through-thickness direction near the hole. It is noteworthy that bearing strength increases reported here for the FFRP architecture are equivalent to z-pin reinforcement, but at much lower reinforcement volume fractions (1% CNTs vs. 4% z-pins) [67], indicating that the aligned CNTs are at least as effective as the z-pins under these criteria.

4. Conclusions and recommendations

Both interlaminar and intralaminar mechanical reinforcement have been demonstrated using aligned-CNTs organized in a three-dimensional hierarchical laminated composite architecture. Significant improvements, comparable to those provided by stitching and z-pinning, are demonstrated for Mode I interlaminar fracture toughness, corresponding to a mechanism of CNT-pull-out toughening via bridging. Bridging is modeled using a closed-form

Please cite this article in press as: Wicks SS et al. Interlaminar and intralaminar reinforcement of composite laminates with aligned carbon nanotubes. Compos Sci Technol (2009), doi:10.1016/j.compscitech.2009.09.001

solution and populated by observed CNT pull-out lengths in the fracture surfaces. The model is found to predict the overall magnitude of the toughness enhancement due to the nanostructured reinforcement, given nominal and observed input properties, and the dependence of toughening on these input parameters quantified via parametric study. The magnitude of predicted toughening is strongly dependent on CNT pull-out length, and is limited by the strength of the reinforcing CNTs (i.e., the CNTs may break before pull-out, providing little toughness enhancement). Taken along with the tension-bearing testing results, substantial improvement in both in-plane and through-thickness reinforcement due to the aligned CNTs is observed. The magnitude of the improvement in strength and toughness due to the aligned CNTs is comparable or greater than z-pinning or stitching at comparable reinforcement densities, as predicted by the model due to the scale-dependence of toughness. The concomitant increase in tension-bearing stiffness and strengths, along with the interlaminar enhancement is noteworthy because z-pinning and stitching typically *decrease* in-plane properties due to damage (fiber waviness, crimping, and breakage; resin-rich areas; cure stresses and microcracking; swelling and reduced fiber volume content) created during insertion [12,22]. Aligned CNTs in the FFRP simply reside between the existing fibers, and no insertion damage arises.

Areas for future research in the area of aligned-CNT reinforced advanced composites are numerous and include: additional mechanical characterizations, especially toughness (Mode II, where z-pinning and stitching are particularly ineffective), impact resistance, and damage tolerance; determination of any additional toughening mechanisms at the interface beyond CNT bridging; modeling of the multi-scale elastic and damage response for these systems (some work has appeared recently [68]); multifunctional property testing, such as electrical and thermal conductivities (some work has appeared in this area, e.g., [69]); development of other fabrication routes beyond hand layup for the FFRP system; replication of the FFRP architecture using carbon fibers, where CNT growth on the carbon fibers must be shown to maintain fiber tensile properties; and other topics such as continuous rather than batch production of aligned CNTs, and particle exposure studies during the fabrication and machining of CNT-containing laminates such as the FFRP [70–72].

Acknowledgements

This work was supported by Airbus S.A.S., Boeing, Embraer, Lockheed Martin, Saab AB, Sprit AeroSystems, Textron Inc., Composite Systems Technology, and TohoTenax through MIT's Nano-Engineered Composite aerospace STructures (NECST) Consortium. The authors thank Namiko Yamamoto (MIT) for extensive fabrication instruction and general assistance, Derreck Barber (MIT) and Megan Tsai (MIT) for fabrication assistance, Dr. Stephen P. Engelstad and Robert W. Koon (Lockheed Martin) for tension-bearing testing and analysis assistance, and John Kane and the entire Technology Laboratory for Advanced Materials and Structures (TELAMS) at MIT for technical support and advice.

References

[1] Thostenson ET, Ren Z, Chou T-W. Advances in the science and technology of carbon nanotubes and their composites: a review. Compos Sci Technol 2001;61(13):1899–912.
[2] Coleman JN, Khan U, Blau WJ, Gun'ko YK. Small but strong: a review of the mechanical properties of carbon nanotube–polymer composites. Carbon 2006;44(9):1624–52.
[3] Ajayan PM, Tour JM. Materials science: nanotube composites. Nature 2007;447(7148):1066–8.
[4] Thostenson ET, Li C, Chou T-W. Nanocomposites in context. Compos Sci Technol 2005;65(3–4):491–516.
[5] Schulte K, Windle AH. Special issue: carbon nanotube (CNT) – polymer composites. Compos Sci Technol 2007;67(5):777.
[6] Lavine M. The right combination. Science 2006;314(5802):1099.
[7] Garcia EJ, Hart AJ, Wardle BL, Slocum A. Fabrication and testing of long carbon nanotubes grown on the surface of fibers for hybrid composites. In: 47th AIAA/ASME/ASCE/AJS/ASC structures, structural dynamics, and materials conference proceedings. Newport, RI, May 1–4, 2006.
[8] Garcia EJ, Hart JA, Wardle BL. Long carbon nanotubes grown on the surface of fibers for hybrid composites. AIAA J 2008;46(6):1405–12.
[9] Garcia EJ, Wardle BL, Hart AJ. Joining prepreg composite interfaces with aligned carbon nanotubes. Compos Part A 2008;39:1065–70.
[10] Garcia EJ, Wardle BL, Hart AJ, Yamamoto N. Fabrication and multifunctional properties of a hybrid laminate with aligned carbon nanotubes grown in situ. Compos Sci Technol 2008;68(9):2034–41.
[11] Wardle BL. Nanocomposites and nano-engineered composites reinforced with aligned carbon nanotubes. In: 17th international conference on composite materials proceedings. Edinburgh, Scotland, July 27–31, 2009.
[12] Tong L, Mouritz AP, Bannister MK. 3D Fibre reinforced polymer composites. Oxford; 2002.
[13] Tsotsis TK, Markus, A, editors. AST composite wing program work Unit IV-design, analysis, and manufacturing studies. NASA/CR-1999-NAS1-20546. The Boeing Company, Long Beach, CA; December, 1999.
[14] Larsson F. Damage tolerance of a stitched carbon/epoxy laminate. Compos Part A: Appl Sci Manuf 1997;28(11):923–34.
[15] Dransfield KA, Jain LK, Mai Y-W. On the effects of stitching in CFRPs – I. Mode I delamination toughness. Compos Sci Technol 1998;58(6):815–27.
[16] Partridge IK, Cartié DDR. Delamination resistant laminates by Z-Fiber® pinning: part I manufacture and fracture performance. Compos Part A: Appl Sci Manuf 2005;36(1):55–64.
[17] Sharma SK, Sankar BV. Effect of stitching on impact and interlaminar properties of graphite/epoxy laminates. J Thermoplast Compos Mater 1997;10(3):241–53.
[18] Mouritz AP, Leong KH, Herszberg I. A review of the effect of stitching on the in-plane mechanical properties of fibre-reinforced polymer composites. Compos Part A: Appl Sci Manuf 1997;28(12):979–91.
[19] Reeder JR. Stitching vs. a toughened matrix: compression strength effects. J Compos Mater 1995;29(18):2464–87.
[20] Zhang X, Hounslow L, Grassi M. The influence of Z-pinning on low-velocity impact and post-impact performance of laminated carbon composites. In: 14th International conference on composite materials (ICCM-14) proceedings, San Diego, CA; 2003.
[21] Steeves CA, Fleck NA. In-plane properties of composite laminates with through-thickness pin reinforcement. Int J Solids Struct 2006;43(10):3197–212.
[22] Mouritz AP. Review of z-pinned composite laminates. Compos Part A: Appl Sci Manuf 2007;38(12):2383–97.
[23] Gojny FH et al. Carbon nanotube-reinforced epoxy-composites: enhanced stiffness and fracture toughness at low nanotube content. Compos Sci Technol 2004;64(15):2363–71.
[24] Qiu J, Zhang C, Wang B, Liang R. Carbon nanotube integrated multifunctional multiscale composites. Nanotechnology 2007;18(27):275708.
[25] Bekyarova E, Thostenson ET, Yu A, Kim H, Gao J, Tang J, et al. Multiscale carbon nanotube-carbon fiber reinforcement for advanced epoxy composites. Langmuir 2007;23(7):3970–4.
[26] Bekyarova E et al. Functionalized single-walled carbon nanotubes for carbon fiber–epoxy composites. J Phys Chem C 2007;111:17865–71.
[27] Veedu VP et al. Multifunctional composites using reinforced laminae with carbon-nanotube forests. Nat Mater 2006;5(6):457–62.
[28] Zhu J et al. Processing a glass fiber reinforced vinyl ester composite with nanotube enhancement of interlaminar shear strength. Compos Sci Technol 2007;67(7–8):1509–17.
[29] Dzenis Y. Materials science: structural nanocomposites. Science 2008;319(5862):419–20.
[30] Adhikari K HP, Simard B, Johnston A. Effect of the localized application of SWNT modified epoxy on the interlaminar shear strength of carbon fiber laminates. In: 47th AIAA structures, dynamics, and materials conference proceedings, Newport, RI, May 1–4, 2006.
[31] Thakre PR LD, Zhu J, Barrera EV. Processing and characterization of epoxy-SWCNT-woven fabric composites. In: 47th AIAA structures, dynamics, and materials conference proceedings. Newport, RI, May 1–4, 2006.
[32] Qian H et al. Hierarchical composites reinforced with carbon nanotube grafted fibers: the potential assessed at the single fiber level. Chem Mater 2008;20(5):1862–9.
[33] Sager RJ et al. Effect of carbon nanotubes on the interfacial shear strength of T650 carbon fiber in an epoxy matrix. Compos Sci Technol 2009;69(7–8):898–904.
[34] Kepple KL et al. Improved fracture toughness of carbon fiber composite functionalized with multi walled carbon nanotubes. Carbon 2008;46(15):2026–33.
[35] Mathur RB, Chatterjee S, Singh BP. Growth of carbon nanotubes on carbon fibre substrates to produce hybrid/phenolic composites with improved mechanical properties. Compos Sci Technol 2008;68(7–8):1608–15.
[36] Yamamoto N et al. High-yield growth and morphology control of aligned carbon nanotubes on ceramic fibers for multifunctional enhancement of structural composites. Carbon 2008.
[37] Blanco J, Garcia EJ, Guzman deVilloria R, Wardle BL. Limiting mechanisms in mode I interlaminar toughness of composites reinforced with aligned carbon nanotubes. J Compos Mater 2009;43(8).

Please cite this article in press as: Wicks SS et al. Interlaminar and intralaminar reinforcement of composite laminates with aligned carbon nanotubes. Compos Sci Technol (2009), doi:10.1016/j.compscitech.2009.09.001

[38] Thoppul SD, Finegan J, Gibson RF. Mechanics of mechanically fastened joints in polymer–matrix composite structures – a review. Compos Sci Technol 2009;69(3–4):301–29.
[39] Gu YH. Fracture behavior of continuous alumina fiber reinforced epoxy. J Compos Mater 1994;28(13):1227–36.
[40] Hogg PJ. Composites in armor. Science 2006;314(5802):1100–1.
[41] Garcia EJ, Hart AJ, Wardle BL, Slocum AH. Fabrication of composite microstructures by capillarity-driven wetting of aligned carbon nanotubes with polymers. Nanotechnology 2007;18(16):165602.
[42] Ishiguro K, et al. Processing and characterization of infusion-processed hybrid composites with in situ grown aligned carbon nanotubes. In: 50th AIAA structures, structural dynamics, and materials conference proceedings, Palm Springs, CA, May 4–7, 2009.
[43] Ishiguro K, et al. Manufacturing process for 3D nano-engineered composite materials with aligned carbon nanotubes grown in situ. In: 24th American society for composites (ASC) technical conference proceedings. Univ of Delaware, September 15–17, 2009.
[44] Sun X, Wood MDK, Tong L. A parametric study on the design of stitched laminated DCB specimens. In: Composite structures 13th international conference on composite structures – ICCS/13, vol. 75, Nos. 1–4; 2006. p. 72–8.
[45] Soni SR, Freels J, Kuhn J. Mode I failure in Z-pinned co-cured laminated composites. In: 40th International SAMPE technical conference proceedings, Memphis, TN, Sep 8–11, 2008.
[46] ASTM, D5528-01. Standard test method for Mode I interlaminar fracture toughness of unidirectional fiber-reinforced polymer matrix composites; 2002.
[47] Adams DF, Carlsson LA, Pipes RB. Experimental characterization of advanced composite materials. Boca Raton: CRC Press; 2003.
[48] ASTM D 5961/D 5961M-08. Standard test method for bearing response of polymer matrix composite laminates; 2008.
[49] Kim J-K, Sham M-L. Impact and delamination failure of woven–fabric composites. Compos Sci Technol 2000;60(5):745–61.
[50] Wei Zhang et al. Heterogeneity in epoxy nanocomposites initiates crazing: significant improvements in fatigue resistance and toughening. Small 2009;5(12):1403–7.
[51] Tong L, Tan P, Sun X. Effect of long multi-walled carbon nanotubes on delamination toughness of laminated composites. J Compos Mater 2008;42(1):5–23.
[52] Garcia EJ et al. Aligned carbon nanotube reinforcement of graphite/epoxy ply interfaces. In: 16th International conference on composite materials (ICCM) proceedings, Kyoto, Japan, July 8–13, 2007.
[53] Deng F, Ogasawara T, Takeda N. Investigation of the deformation mechanics in carbon nanotubes–polymer composites at microscopic and atomistic level. In: 16th International conference of composites materials proceedings, Kyoko, Japan.
[54] Yu M-F et al. Strength and breaking mechanism of multiwalled carbon nanotubes under tensile load. Science 2000;287(5453):637–40.
[55] Chen J et al. The structural evolution of thin multi-walled carbon nanotubes during isothermal annealing. Carbon 2007;45(2):274–80.
[56] Zhang S et al. Mechanics of defects in carbon nanotubes: atomistic and multiscale simulations. Phys Rev B 2005;71(11):115403.
[57] Xu Z, Wang L, Zheng Q. Enhanced mechanical properties of prestressed multi-walled carbon nanotubes. Small 2008;4(6):733–7.
[58] Fisher FT, Bradshaw RD, Brinson LC. Effects of nanotube waviness on the modulus of nanotube-reinforced polymers. Appl Phys Lett 2002;80(24):4647–9.
[59] Cebeci H, Guzman deVilloria R, Hart AJ, Wardle BL. multifunctional properties of high volume fraction aligned carbon nanotube polymer composites with controlled morphology. Compos Sci Technol, submitted for publication.
[60] Tercan M, Asi O, Aktas A. An experimental investigation of the bearing strength of weft-knitted 1×1 rib glass fiber composites. Compos Struct 2007;78(3):392–6.
[61] Matthews FL, Roshan AA, Phillips LN. The bolt bearing strength of glass/carbon hybrid composites. Composites 1982;13(3):225–7.
[62] Chen J-C, Lu C-K, Chiu C-H, Chin H. On the influence of weave structure on pin-loaded strength of orthogonal 3D composites. Composites 1994;25(4):251–62.
[63] Wang D, Chen G, Li Z, Kou C. Bearing strength analysis of single mechanically fastened joint in stitched laminates. J Reinf Plast Compos 2006;25(7):711–24.
[64] Xiao Y, Ishikawa T. Bearing strength and failure behavior of bolted composite joints (part I: experimental investigation). Compos Sci Technol 2005;65(7–8):1022–31.
[65] Dickinson LC, Farley GL, Hinders MK. Prediction of effective three-dimensional elastic constants of translaminar reinforced composites. J Compos Mater 1999;33(11):1002–29.
[66] Grassi M, Zhang X, Meo M. Prediction of stiffness and stresses in z-fibre reinforced composite laminates. Compos Part A: Appl Sci Manuf 2002;33(12):1653–64.
[67] Li R et al. Improving bearing performance of composite bolted joints using z-pins. Compos Sci Technol 2009;69(7–8):883–9.
[68] Ray MC, Guzman deVilloria R, Wardle BL. Load transfer analysis in short carbon fibers with radially-aligned carbon nanotubes embedded in a polymer matrix. J Appl Mech 2009. in press.
[69] Yamamoto N, Garcia EJ, Wardle BL, Hart AJ. Thermal and electrical properties of hybrid woven composites reinforced with aligned carbon nanotubes. In: 49th AIAA structures, dynamics, and materials conference proceedings, Schaumburg, IL, April, 7–10, 2008.
[70] Bello DB, et al. Exposures to nanoscale particles and fibers during handling, processing, and machining of nanocomposites and nano-engineered composites reinforced with aligned carbon nanotubes. In: 17th International conference on composite materials (ICCM) proceedings, Edinburgh, Scotland, July 27–31, 2009.
[71] Bello D et al. Particle exposure levels during CVD growth and subsequent handling of vertically-aligned carbon nanotube films. Carbon 2008;46(6):974–7.
[72] Bello D et al. Exposure to nanoscale particles and fibers during machining of hybrid advanced composites containing carbon nanotubes. J Nanopart Res 2008;11(1):231–49.

Please cite this article in press as: Wicks SS et al. Interlaminar and intralaminar reinforcement of composite laminates with aligned carbon nanotubes. Compos Sci Technol (2009), doi:10.1016/j.compscitech.2009.09.001